Epitaxy and exfoliation of free-standing Heusler membranes using a graphene interlayer

Dongxue Du,[1] Sebastian Manzo,[1] Chenyu Zhang,[1] Vivek Saraswat,[1]
Michael S. Arnold,[1] Paul M. Voyles,[1] and Jason K. Kawasaki[1]

[1] *Materials Science and Engineering, University of Wisconsin-Madison, Madison, WI 53706*

(Dated: June 19, 2020)

Single-crystalline membranes of functional materials enable the tuning of properties via extreme strain states; however, conventional routes for producing membranes require the use of sacrificial layers and chemical etchants, which can both damage and limit the ability to make membranes ultrathin. Here we demonstrate the epitaxial growth of cubic and hexagonal Heusler compounds on graphene-terminated Al_2O_3 substrates. The weak Van der Waals interactions of graphene enable the mechanical exfoliation of LaPtSb and GdPtSb films to yield free-standing membranes. Despite the presence of the graphene interlayer, the Heusler films have epitaxial registry to the underlying sapphire, as revealed by x-ray diffraction, reflection high energy electron diffraction, and transmission electron microscopy. Some films show a uniform in-plane rotation of several degrees with respect to the substrate, which we attribute to a combination of lattice mismatch and weakened Heusler film / sapphire substrate interactions through graphene. The residual resistivity of semi free-standing films on graphene-terminated substrates is similar to the residual resistivity of films grown by direct epitaxy. Our graphene-mediated approach provides a promising platform for tuning the magnetic, topological, and multiferroic properties of Heuslers in a clean, single-crystalline membrane system.

I. INTRODUCTION

Membranes are a powerful platform for flexible devices and for tuning properties via strain [1–7]. In contrast to static epitaxial strain, the strain applied to free-standing membranes is more tuneable since it can be applied dynamically, anisotropically, and at larger magnitudes. For example, recent experiments on ultrathin oxide membranes demonstrate the application of extreme uniaxial strain of 8% [1], whereas the maximum strain possible in an epitaxial thin film is typically no more than 3% before plastic deformation. Methods for making single-crystalline membranes of semiconductors are well established and typically rely on the etching of a sacrificial buffer layer. This strategy has been used to fabricate free standing membranes of GaAs [2], Si [3, 4], SiGe [5]. A similar approach has recently been applied to transition metal oxides, using a water-soluble layer [1, 8]. However, these chemically selective etch approaches are not universally applicable and require detailed knowledge of the etch chemsitry. Moreover, ultrathin films and membranes, which are required for achieving extreme strain states, can be extremely sensitive to air exposure due to the high surface to volume ratio. Therefore, it is important to develop alternative, etch-free methods for synthesizing single-crystalline membranes of functional materials.

Heusler compounds are multifunctional intermetallic materials, for which little is known about etch chemistries. These materials have highly tunable magnetic [9], electronic [10, 11], ferroelastic [12–14], and topological properties [15–19]. For example, cubic GdPtBi is an antiferromagentic Weyl semimetal whose band inversion strength is sensitive to strain [15, 20, 21], LaPtSb is a polar metal [22], and LuPtBi and YPtBi are promising candidates for topological superconductivity [23, 24]. Although single-crystalline 90 nm thick Heusler membranes have previously been fabricated using sacrificial semiconductor etch layers [13], manipulating the properties induced by extreme strain states in ultrathin membranes will require new etch-free synthesis strategies. Recently, "remote epitaxy" has emerged as an alternative strategy for synthesizing single-crystalline free-standing semiconductor [25, 26], oxide [27], and halide perovskite [28] membranes. In this growth mode, growth on a graphene terminated substrate yields a film with epitaxial registry to the underlying substrate, despite the screening effects from graphene. The weak Van der Waals interactions between film and graphene enable semiconductor or oxide membranes to be exfoliated using a metal stressor layer. However, it remains an open question whether a similar growth and exfoliation mechanism can be applied to other materials systems such as intermetallic compounds, which have more covalent or metallic bonding character than ionically bonded compound semiconductors and oxides [26].

Here we demonstrate an etch-free method of synthesizing epitaxial Heusler films on a graphene-terminated single crystalline substrate. These films can be mechanically exfoliated using thermal release tape to yield a free-standing Heusler membrane, without the need for a metal stressor layer. We demonstrate the epitaxial growth of hexagonal LaPtSb and cubic GdPtSb on monolayer graphene/Al_2O_3 (0001). Despite the presence of graphene, the *R*PtSb (R = La or Gd) films have epitaxial registry to the underlying sapphire substrate. The weak Van der Waals decoupling between *R*PtSb film and sapphire substrate drives two unique aspects that have not been observed in oxide or semiconductor "remote epitaxy" systems: (1) the *R*PtSb membranes can be mechanically exfoliated without the need for a metal

stressor layer or etchants, and (2) in some samples an in-plane twist is observed between the *R*PtSb film and the sapphire substrate. Because of these weakened interactions, films grown on graphene/Al_2O_3 can be described as *semi* free-standing membranes. We discuss possible mechanisms for the growth on graphene and the observed in-plane twist, which may arise from a combination of lattice mismatch and weakened interactions between *R*PtSb and sapphire. The spontaneous twist suggests a potential bottom-up method of creating Moire heterostructures from pseudo two-dimensional materials. Unstrained, semi free-standing membranes grown on graphene-terminated sapphire have similar residual resistivity as films grown by direct epitaxy without graphene, indicating similar quality. This work provides a new approach for making free-standing membranes of topological and magnetic Heusler materials, without the need for etchants or stressor layers.

II. RESULTS

Concept. We first describe the crystallographic relationships that are possible in the cubic and hexagonal Heusler / graphene / Al_2O_3 system. Figs. 1(a,b) show schematic crystal structures of the LaPtSb ($P6_3mc$) and GdPtSb ($F\bar{4}3m$) films on graphene/Al_2O_3 (0001). In both systems, the closest lattice match is expected between the *R*PtSb films and the sapphire substrate, rather than *R*PtSb and graphene. For LaPtSb on sapphire, the lattice mismatch is $(a_{Al_2O_3} - a_{LaPtSb})/a_{Al_2O_3} = 4.20\%$. For (111)-oriented GdPtSb on (0001) sapphire, the lattice mismatch is $(a_{Al_2O_3} - \frac{1}{2}d_{110,GdPtSb})/a_{Al_2O_3} = 2.73\%$. Since the layer transferred graphene has random polycrystalline domains, if the primary interactions are between *R*PtSb film and graphene, then a polycrystalline film is expected. If, on the other hand, the primary interactions are between *R*PtSb film and the underlying substrate, then an epitaxial film is expected. Given the recent demonstration of semi-*lattice transparency* of graphene during GaAs/graphene/GaAs "remote epitaxy" [25], we expect epitaxial registry between *R*PtSb and the underlying sapphire to dominate.

Epitaxial growth and in-situ diffraction. Polycrystalline monolayer graphene (typical domain size $\sim 10-20\ \mu$m) was grown on copper foils by chemical vapor deposition, and then transferred by wet chemical methods to single crystalline Al_2O_3 (0001) substrates, using a polymethyl methacrylate (PMMA) handle (Methods). Figs. 1(f) and (g) show the Raman spectrum and atomic force microscopy (AFM) topography of the graphene on Al_2O_3. In the Raman spectrum, the sharp *G* and 2*D* modes (FWHM of 2D-band is $\sim$23 cm^{-1}), and the negligible D-band intensity, indicate a clean transfer with minimal point defects in the graphene [29–32]. In the AFM image, we observe a step-and-terrace morphology of the underlying sapphire, along with wrinkles in the graphene that appear as bright streaks. AFM images

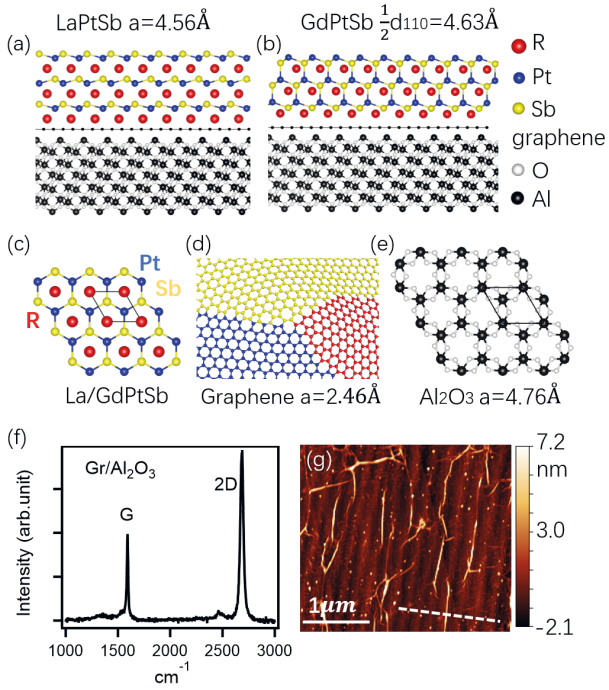

FIG. 1. **Concept for epitaxial growth of Heusler compounds on graphene/Al_2O_3.** (a) Schematic cross sectional crystal structure of hexagonal (0001)-oriented LaPtSb on graphene/Al_2O_3 (0001). (b) Cubic (111)-oriented GdPtSb on graphene/Al_2O_3 (0001). Both (a) and (b) are viewed down a $[11\bar{2}0]$ zone axis of Al_2O_3. (c-e) In-plane crystal structures of *R*PtSb, polycrystalline graphene, and Al_2O_3 substrate. (f) Raman spectrum of graphene after layer transfer to Al_2O_3. (g) AFM image of graphene on Al_2O_3. The dashed line marks the position of the AFM line cut in Fig. s1.

at this length scale reveal no obvious tears; however, we cannot rule out tears or pinholes at a length scale of down to $\sim$ 10 nm, which is typical for CVD-grown graphene [33, 34]. Additional defects are expected to result from the transfer process to the Al_2O_3 substrate.

Following graphene layer transfer, the graphene/Al_2O_3 samples follow a sequence of anneals up to 700 °C in ultrahigh vacuum (pressure less than 2×10^{-10} Torr, see Methods). At this stage the reflection high energy electron diffraction (RHEED) pattern shows a bright but diffuse specular reflection compared to bare sapphire [22], which we attribute to diffuse scattering from the randomly oriented top graphene layer. There are weak diffraction streaks at the +1 and −1 positions (arrows), which we attribute to the underlying sapphire substrate (Fig. 2(a1)).

30-40 nm thick LaPtSb and GdPtSb films were grown by molecular beam epitaxy (MBE) on the graphene/Al_2O_3 at 600 °C, using conditions similar to Ref. [22] (Methods). RHEED patterns for both LaPtSb and GdPtSb indicate growth with epitaxial registry to the underlying sapphire substrate. For LaPtSb (Figs. 2(a2,b2)), the RHEED patterns are sharp and streaky

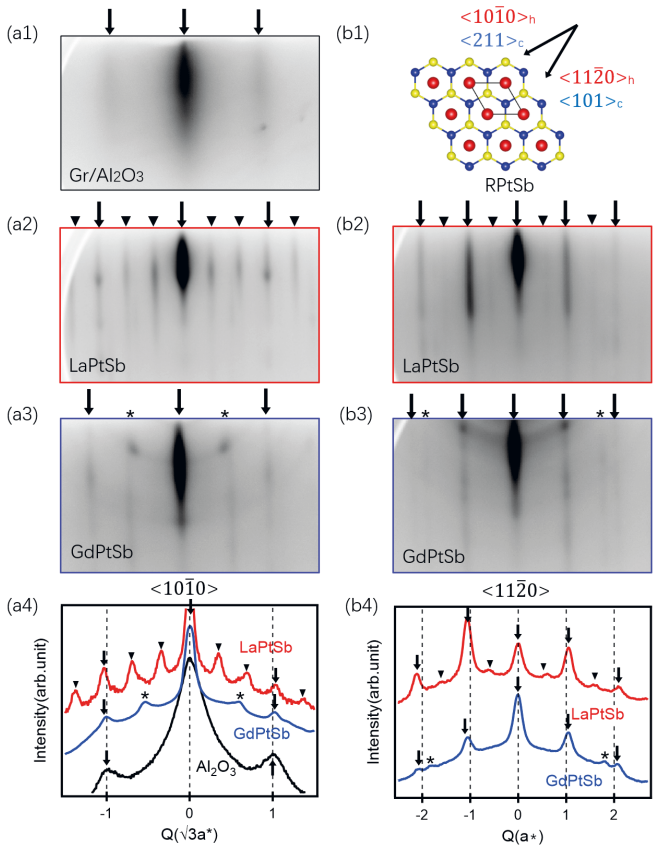

FIG. 2. **In-situ electron diffraction tracking the growth of LaPtSb and GdPtSb on graphene/Al_2O_3(0001).** Left column: electron beam oriented along $\langle 10\bar{1}0\rangle_{Al_2O_3}$. Right column: beam oriented along $\langle 11\bar{2}0\rangle_{Al_2O_3}$. (a1) Reflection high-energy electron diffraction (RHEED) pattern of graphene on Al_2O_3 after a 700 °C anneal. Black arrows mark the underlying Al_2O_3 reflections. (b1) Crystal structure. In the crystallographic direction labels, h indicates a hexagonal basis (for LaPtSb) and c indicates a cubic basis (for GdPtSb). (a2, b2) RHEED patterns for the LaPtSb film. Black arrows mark the bulk reflections, black triangles mark superstructure reflections, corresponding to a well ordered (2×3) surface reconstruction. (a3, b3) GdPtSb on graphene/Al_2O_3. In addition to the expected bulk reflections (black arrows), additional reflections are observed that correspond to a second domain rotated by 30 degrees (black asterisks). (a4, b4) Intensity lines cuts of the RHEED patterns. The ΔQ spacings for the secondary reflections of GdPtSb (asterisks) differ from the primary reflections (arrows) by a factor of $\sqrt{3}$, consistent with a 30 degree in-plane rotation.

with a well ordered (2×3) surface reconstruction, as indicate by the clear 1/2 and 1/3-order reflections (black triangles). This is the same reconstruction observed for LaPtSb grown by direct epitaxy on Al_2O_3 [22]. No other crystallographic domains or secondary phases are observed for LaPtSb by RHEED.

For GdPtSb [Figs. 2(a3,b3)], the RHEED patterns are not as sharp as LaPtSb, and show hints of two domains that are related by an in-plane rotation of 30 degrees. For beam oriented along the $\langle 10\bar{1}0\rangle$ azimuth of the sapphire substrate, in addition to the expected reflections at a ΔQ spacing of $\sqrt{3}a^*$ (black arrows in Fig. 2(a3), a^* is the reciprocal lattice constant of Al_2O_3), we observe a second set of streaks at spacing at $\Delta Q \approx a^*$ (black asterisks). Similarly, for RHEED beam oriented along the $\langle 11\bar{2}0\rangle$ azimuth of sapphire [Fig. 2(b3)], in addition to the expected streaks at spacing $\Delta Q = a^*$, we observe a set of reflections with spacing $\Delta Q = \sqrt{3}a^*$ (black asterisks). The additional reflections suggest the presence of sets two domains: one domain with the expected $\langle 101\rangle_{GdPtSb} \parallel \langle 11\bar{2}0\rangle_{Al_2O_3}$ epitaxial relationship, and the other rotated by ±30 degrees around the Al_2O_3 [0001] axis ($\langle 101\rangle_{GdPtSb} \parallel \langle 10\bar{1}0\rangle_{Al_2O_3}$).

The XRD θ-2θ scans for both LaPtSb and GdPtSb on graphene/Al_2O_3 in Fig. 3 (black traces) confirm epitaxial growth with the expected LaPtSb (0001) and GdPtSb (111) out of plane orientations, respectively. For LaPtSb, only the $000l$ reflections are detected in the θ-2θ scan. The rocking curve width of the LaPtSb 0002 reflection is 18.8 arc sec (Fig. s2(a)), larger than the 6.7 arc sec width of films grown directly on sapphire [22]. The XRD $\theta - 2\theta$ scan for GdPtSb is similarly characterized by strong (111)-type reflections, with the addition of a small impurity phase reflection at 2θ=55.9° that we attribute to Gd_3Pt (space group Pnma). In spite of the small amount of impurity phase, the GdPtSb sample also has good crystalline quality, which is confirmed by the 15.422 arcsecond FWHM of the 111 reflection extracted from the rocking curve in Fig. s2(b).

Membrane exfoliation. Heusler films grown on graphene/Al_2O_3 can be exfoliated to yield free-standing membranes, using thermal release tape and no secondary metal stressor layer. To perform the exfoliation, we adhere the sample substrate-side down on a glass slide using Ted Pella Crystalbond 509. Then we stick thermal release tape on the film surface evenly. The membrane is exfoliated by quickly tearing off the tape. Fig. 3 (red and blue traces) show $\theta - 2\theta$ scans of exfoliated LaPtSb and GdPtSb membranes, after placing the membrane on a rigid secondary substrate for ease of XRD measurements. For the LaPtSb membrane exfoliated and placed on Si (111) (Fig. 3(a) red curve) we observe all of the expected 0002, 0004, and 0006 reflections from the LaPtSb membrane. For the GdPtSb exfoliated and placed onto a glass slide (Fig. 3(b), blue curve), we observe only the 111 reflection. The 222 and 333 reflections are too weak to be observed, which we attribute to their relatively low structure factors and to challenges in sample alignment to a thin membrane. As a control, we attempted the exfoliation of Heusler films grown directly on Al_2O_3 without graphene, which could not be successfully exfoliated using thermal release tape. An important aspect of this system is that unlike the compound semiconductor [25] or oxide [27] systems grown by "remote epitaxy," in this Heusler/graphene/Al_2O_3 system, no metal stressor layer was required in order to perform the exfoliation. We note, however, that the exfoliation has not yet been op-

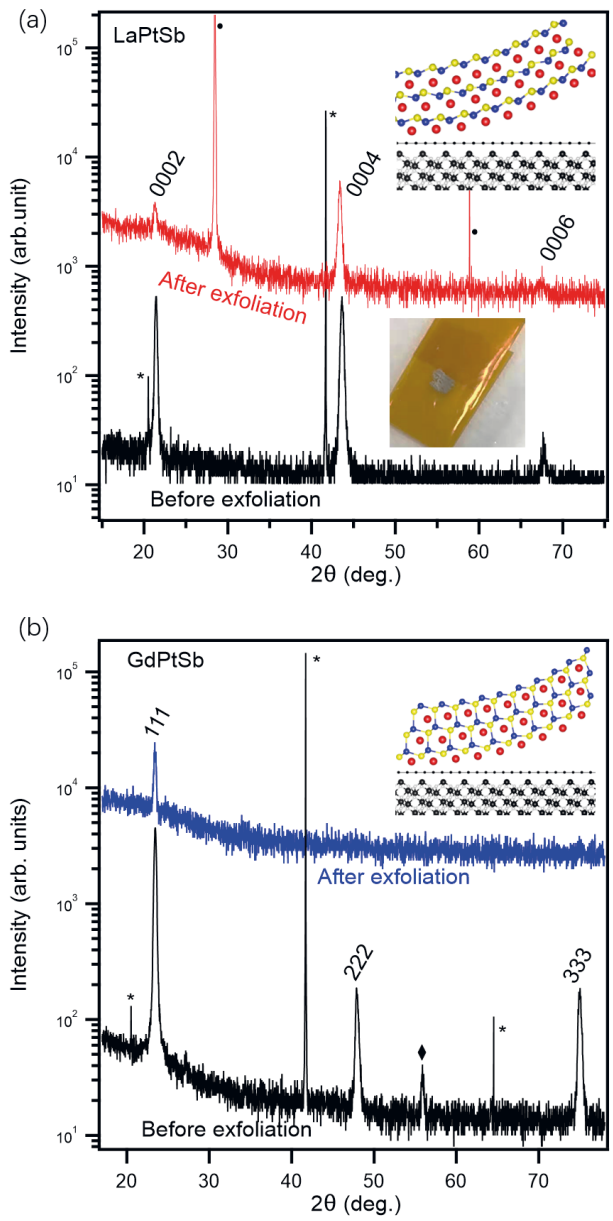

FIG. 3. **Crystallography and exfoliation of LaPtSb and GdPtSb membranes.** (a) XRD θ-2θ (Cu $K\alpha$) scans before exfoliation (black, on sapphire substrate) and after exfoliation (red, transferred to Si dummy substrate). Sapphire substrate reflections are marked by asterisks and Si reflections are marked by closed circles. In the film and exfoliated membrane, only $(000l)$-type reflections are observed indicating a single-crystalline film. (b) θ-2θ scans of GdPtSb before (black curve, on sapphire substrate) and after exfoliation (blue curve, on glass slide). In addition to the epitaxial (lll)-type reflections, a small impurity phase of Gd_3Pt (Pnma) is observed and marked with a diamond.

timized and there are typically tears around hundreds of microns apart over a 5×5 mm^2 sample. These results demonstrate that Heusler/graphene/sapphire structures provide a straightforward path for creating free-standing Heusler membranes.

Rotations and twist in *semi* free-standing membranes. XRD pole figure measurements before exfoliation confirm that the *R*PtSb films adopt epitaxial registry with the Al_2O_3 substrate; however, in-plane rotations are observed that do not appear for direct epitaxy on Al_2O_3, without the graphene [22]. We first focus on LaPtSb on graphene/Al_2O_3. Fig. 4(a) shows in-plane rotation (ϕ) scans of the LaPtSb $10\bar{1}2$ reflection and the Al_2O_3 $10\bar{1}4$ reflection. The LaPtSb $10\bar{1}2$ reflection shows the expected six-fold symmetry and only a single domain is observed, as expected for epitaxy between LaPtSb and sapphire. However, closer inspection reveals that the singly oriented LaPtSb film (or semi-free-standing membrane) is rotated in-plane by 3.2 degrees around the Al_2O_3 [0001] axis. LaPtSb films grown by direct epitaxy on Al_2O_3 do not show this rotation (Fig. s3(b) or [22]).

The GdPtSb film on graphene/Al2O$_3$ shows two sets of domains, one with the GdPtSb 220 aligned with the Al_2O_3 $10\bar{1}4$ ($\Delta\Phi_0 = 0°$), corresponding to the expected $\langle 101\rangle_{GdPtSb} \parallel \langle 11\bar{2}0\rangle_{Al_2O_3}$ relationship, and the other set rotated by ± 30 degrees (Fig. 4(b)). In contrast, GdPtSb films grown directly on sapphire do not show the ± 30 degree domains (Supplemental Materials Fig. s3(a)). Annular bright field (ABF) scanning transmission electron microscopy (STEM) images in Figs. 4(c,d) confirm the existence of these two sets of domains for growth on graphene/Al_2O_3. In these images, the atomic structure is resolved a few nanometers away from the interface, but it is difficult to resolve the registry at the GdPtSb/graphene/sapphire interface. We attribute the blurred interface to partial film delamination during TEM sample preparation, given the previous observation that membranes are easily exfoliated. In Fig. 4(c), the STEM image of the $\Delta\phi_0 = 0$ domain consists of arrays of tilted spindle-shaped dark spots, each of which represents a combination of one Gd atomic column, one Pt atomic column, and one Sb atomic column, as is circled in the inset cartoon structure of GdPtSb viewed from the $\langle 101\rangle$ direction. For the STEM image of the $\pm 30°$ rotated GdPtSb, the spindle-shaped spots are aligned along the vertical direction corresponds to clusters of Gd-Pt-Sb atomic columns, as shown by the inset cartoon of Fig. 4(d).

Several possible origins may explain the 3.2° in-plane twist of LaPtSb and $\pm 30°$ domain formation for GdPtSb, respectively. One possibility is Moire superstructure formation, due the combined lattice mismatch between *R*PtSb film and sapphire, and the weakened film-sapphire interactions due to screening from the graphene interlayer. For LaPtSb, the lattice mismatch with no rotation ($\mathbf{a_{LaPtSb}} \parallel \mathbf{a_{Al_2O_3}}$) is 4.20%. But for the observed in-plane rotation of $\sim 3.2°$, the mismatch is only 0.4% if one considers a 6.9 nm Moire unit cell, in which a (15, 14)

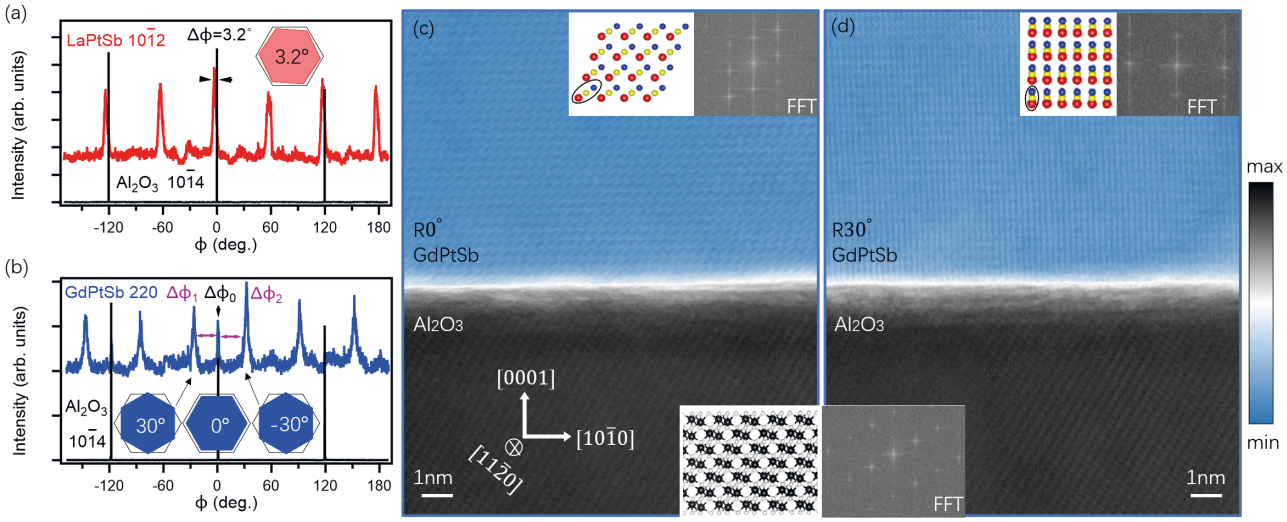

FIG. 4. **Rotations and twist in *semi* free-standing Heusler membranes.** (a) In-plane ϕ scan of LaPtSb $10\bar{1}2$ reflection and Al_2O_3 $10\bar{1}4$ reflections for LaPtSb sample grown on Al_2O_3 with graphene inter-layer before exfoliation. $\Delta\Phi$=3.2° is the in-plane angle between the $\langle 11\bar{2}0\rangle$ direction of LaPtSb and Al_2O_3 substrate. (b) In-plane ϕ scan of GdPtSb 220 reflections and Al_2O_3 $10\bar{1}4$ reflections for GdPtSb sample grown on graphene covered Al_2O_3 before exfoliation. $\Delta\phi_1$=-30° and $\Delta\phi_2$=30° are the in-plane angles between the $\langle 101\rangle$ direction of GdPtSb and the $\langle 11\bar{2}0\rangle$ direction of Al_2O_3 substrate. (c,d) STEM image of the GdPtSb/graphene/Al_2O_3 interface for the two different GdPtSb domains, as viewed along the $\langle 11\bar{2}0\rangle_{Al_2O_3}$ zone axis. We used log scale false-color image to simultaneously visualize the film and substrate for better contrast. The insets show the schematic crystal structures and fast Fourier transforms of the STEM images.

lattice vector of Al_2O_3 is aligned with a $(16, 14)$ lattice vector of LaPtSb [35]. Here, a weak interaction across the graphene changes the balance between the energy of interfacial bonding and the strain energy, favoring small strains via a lattice rotation. Other possible origins include graphene wrinkle formation [36–39] or thermal expansion mismatch [38, 40, 41] during cooldown from the growth temperature of 600 °C to room temperature. Further experiments are required to distinguish the possible origins of twist.

Moire superstructure formation, enabled by the partial screening from graphene, may also explain the ±30° domain formation of GdPtSb. For the $\Delta\phi_0 = 0$ domain with $\langle 101\rangle_{GdPtSb} \parallel \langle 11\bar{2}0\rangle_{Al_2O_3}$ the lattice mismatch is 2.7 %. On the other hand, a ±30° rotation corresponds to a $(3, 3)_{GdPtSb} \parallel (5, 0)_{Al_2O_3}$ superstructure with a mismatach of only −1.5%. Here, we write the GdPtSb lattice vectors in hexagonal coordinates, where $(\mathbf{a}' \parallel 10\bar{1}, \mathbf{b}' \parallel 1\bar{1}0)$. Regardless of the true mechanism of formation, the observed rotations provide a potential route towards the bottom-up synthesis of Moire heterostructures made from three-dimensional materials. To date, the study of Moire bilayers has been limited to two-dimensional materials such as graphene, hexagonal boron nitride, and transition metal dichalcogenides [42–44]. Moire superstructures of new materials offer the potential of tuning electronic bandwidths and the delicate balance between electron-electron repulsion and the kinetic energy, for realization of emergent correlated phases [42].

Electrical transport. Finally, we compare the electrical quality of semi-free-standing membranes grown on graphene/Al_2O_3, versus films grown by direct epitaxy on Al_2O_3. Fig. 5 shows the temperature dependent resistivity of LaPtSb/graphene/Al_2O_3 (red curve) and LaPtSb/Al_2O_3 (black curve). Both samples show a similar residual resistivity (ρ_{2K} = 9.97 and 5.56 $\mu\Omega$·cm, respectively) and similar residual resistivity ratio ($RRR = \rho_{300K}/\rho_{2K}$). Hall effect measurements in a Van der Pauw geometry reveal similar carrier concentrations of $\sim 2 \times 10^{20}$ cm^{-3}. Together, these results suggest that films grown on graphene-terminated sapphire are of similar electrical quality as films grown by direct epitaxy on sapphire.

III. DISCUSSION

Despite our demonstration of Heusler epitaxy on graphene terminated substrates, the microscopic mechanisms for growth and twist in this system are not well understood. One explanation is remote interactions through the graphene, since density functional theory calculations suggest that monolayer graphene only partially screens the underlying lattice potential of most substrates [25, 28]. This "remote epitaxy" mechanism has been used to describe the growth of semiconductor/graphene/semiconductor [25, 26] and oxide/graphene/oxide [27] heterostructures. An alternative

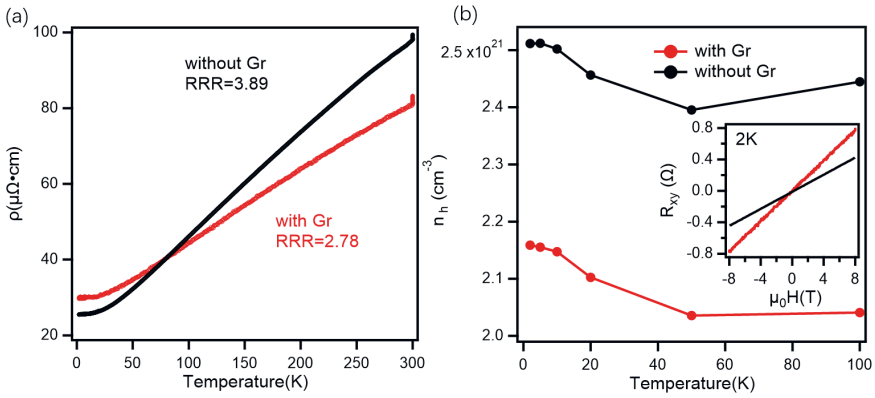

FIG. 5. **Comparison of transport properties between LaPtSb grown on Al_2O_3 with and without graphene.** (a) Resistivity versus temperature. Residual resistivity ratios of them are labeled in the plot. (b) Temperature dependence of carrier concentrations. The inset shows the linear Hall resistance measured at 2K for samples with and without graphene. The data for growth with graphen are colored red and the data for growth without graphene are colored black.

mechanism is the nucleation of Heusler film at pinhole defects of the graphene, i.e. direct epitaxy to exposed regions of the substrate, followed by lateral growth and coalescence. This mechanism is akin to epitaxial lateral overgrowth (ELO), which employs patterned openings in a dielectric mask such as SiO_2 [45–47] or even graphite [48]. Given the $\sim$ 10 nm typical size [33] and $\sim 1\ \mu m^{-2}$ areal density [34] for pinholes in CVD grown graphene (larger defect densities are expected after the transfer and annealing procedure), and the relatively large surface diffusion coefficients for metal adatoms on graphene (up to $D \sim 10^{-6}$ cm^2/s at 300K [49]), in the present Heusler/graphene/Al_2O_3 system we cannot rule out an ELO mechanism. However, the fact that the films can be exfoliated using thermal release tape, without the need for a metal stressor layer, suggests that if pinhole opening are indeed required for epitaxial growth, they do not act as significant anchoring points to inhibit membrane exfoliation. The in-plane twists are also indicative of significant film-substrate decoupling. Further experiments are needed to clarify the epitaxial growth mechanism and the mechanism for spontaneous twist in Heusler/graphene/Al_2O_3.

In summary, we demonstrated the MBE growth of hexagonal and cubic LaPtSb and GdPtSb Heusler films on graphene-terminated Al_2O_3 substrates, followed by exfoliation to yield free-standing membranes. This work expands the range of single-crystalline functional membranes that can be grown by graphene-assisted epitaxy, to include intermetallic compounds that have mixed covalent and metallic bonding. The ease of exfoliation without a stressor layer, and the spontaneous in-plane twists, are unique aspects of this system. This opens the door for tuning of properties via extreme strain states in clean Heusler membranes, and the possibility of tuning bandwidths and correlated phases via Moire twist [42, 50].

IV. ACKNOWLEDGMENTS

Heusler epitaxial film growth and graphene transfers were supported by the Army Research Office (ARO Award number W911NF-17-1-0254) and the National Science Foundation (DMR-1752797). TEM experiments by CZ and PMV were supported by the US Department of Energy, Basic Energy Sciences (DE-FG02-08ER46547) and used facilities supported are by the Wisconsin MRSEC (DMR-1720415). Graphene synthesis and characterization are supported by the U.S. Department of Energy, Office of Science, Basic Energy Sciences, under award no. de-sc0016007. We gratefully acknowledge the use of x-ray diffraction facilities supported by the NSF through the University of Wisconsin Materials Research Science and Engineering Center under Grant No. DMR-1720415.

V. METHODS

A. Synthesis of Graphene

Graphene was grown using thermal chemical vapor deposition of ultra high purity CH_4 at 1050 °C on Cu foil. As-received copper foils (BeanTown Chemical number 145780, 99.8% purity) were cut into 1 inch by 1 inch pieces and soaked in dilute nitric acid (5.7%) for 40 s followed by 3x DI water rinse followed by soaking in acetone and IPA to remove water from the surface. Dilute nitric acid helps remove the oxide and impurity-particles from the surface. Foils were then dried under a gentle stream of air. Foils were subsequently loaded into a horizontal quartz tube furnace in which the furnace can slide over the length of the tube. Prior to monolayer graphene synthesis, the CVD chamber was evacuated to $< 10^2$ Torr using a scroll pump. The system was then back-filled with Ar and H_2, and a steady flow (331 sccm Ar, 9 sccm

H_2) monitored by mass flow controllers was maintained at ambient pressure. The furnace was then slid to surround the samples, and annealed for 30 min. Then 0.3 sccm of P-5 gas (5% CH_4 in Ar) was flowed for 45 min so that a monolayer of graphene formed on the surface. To terminate the growth, the furnace was slid away from the samples, and the portion of the quartz tube containing the samples was cooled to room temperature.

B. Transfer of graphene to Al_2O_3

Our graphene transfer procedure is a modified polymer-assisted wet transfer, similar to the transfer recipes studied in previous works [51]. (0001)-oriented Al_2O_3 substrates were prepared by annealing at 1400°C for 10 hours at atmospheric pressure in order to obtain a smooth, terrace-step morphology. To perform the graphene transfer, the graphene/Cu foils were cut into 5 mm by 5 mm pieces and flattened using clean glass slides. Approximately 300 nm of 495K C2 PMMA (Chlorobenzene base solvent, 2% by wt., MicroChem) was spin coated on the graphene/Cu foil substrate at 2000 RPM for 2 minutes and left to cure at room temperature for 24 hours. Graphene on the backside of the Cu foil was removed via reactive ion etching using 90 W O_2 plasma at a pressure of 100 mTorr for 30 s. The Cu foil was then etched by placing the PMMA/graphene/Cu foil on the surface of an etch solution containing 1-part ammonium persulfate (APS-100, Transene) and 3-parts H_2O. After 10 hours of etching at room temperature, the floating PMMA/graphene membrane was scooped up with a clean glass slide and sequentially transferred into three 30-minute water baths to rinse the etch residuals. The PMMA/graphene membrane was then scooped out of the final water bath using the annealed sapphire substrate, to yield a PMMA/graphene/Al_2O_3 stack.

To remove water at the graphene/Al_2O_3 interface, samples were baked in air at 50°C for 5 minutes, then slowly ramped to 150 °C and baked for another 10 minutes. The PMMA is removed by submerging the sample in an acetone bath at 80°C for 3 hours. This is followed by an isopropanol and water rinse. The sample is indium bonded onto a molybdenum puck and outgassed at 150°C for 1 hour in a loadloack at a pressure $p < 5 \times 10^{-7}$ Torr before introduction to the MBE growth chamber. Finally, the graphene/Al_2O_3 sample is annealed at 400°C for 1 hour in the MBE chamber to desorb remaining organic residues, and then annealed up to 700 °C immediately prior to growth of LaPtSb or GdPtSb.

C. Molecular beam epitaxy of *R*PtSb films

LaPtSb and GdPtSb films were grown on graphene/Al_2O_3 by molecular beam epitaxy (MBE) at a sample temperature of 600°C, using conditions similar to Ref. [22]. La and Gd fluxes were supplied by thermal effusion cells. A mixture of Sb_2 and Sb_1 was supplied by a thermal cracker cell with cracker zone operated at 1200°C. The Pt flux was supplied by an electron beam evaporator. Fluxes were measured in situ using a quartz crystal microbalance (QCM) and calibrated with Rutherford Backscattering Spectroscopy. The R to Pt atomic flux ratio was maintained to be 1:1. Due to the high relative volatility of Sb, *R*PtSb films were grown in an Sb adsorption-controlled regime with a 30% excess Sb flux. 30 nm of GdPtSb and 40 nm of LaPtSb were grown. After the growth, 100 nm amorphous Ge (from an effusion cell) was capped in-situ at room temperature to protect the surfaces from oxidation.

D. Raman and atomic force microscopy of graphene/Al_2O_3

Graphene transfer coverage and cleanliness is studied using field emission scanning electron microscopy (SEM) (Zeiss LEO 1530 Gemini). The graphene quality after the transfer is assessed via Raman spectroscopy using a 532 nm wavelength laser (Thermo Scientific DXR Raman Microscope). The laser power is kept below 5 mW in order to prevent damage to the graphene. The terrace step-morphology of the annealed sapphire substrates with and without graphene termination is analyzed by AFM (Bruker Multimode 8 SPM) in tapping mode.

E. Scanning Transmission Electron Microscopy

The GaPtSb/graphene/Al_2O_3 sample was prepared for TEM using a Zeiss Auriga focused ion beam (FIB) with a final FIB polishing step with a 5 kV 100 pA Ga-ion beam. The sample surface was further polished for a higher smoothness in a Fishione 1040 Nanomill with a 900 eV Ar ion beam, to a thickness of approximately 80 nm. We did not seek to get the thinnest possible sample, as the film layer could peel off from the substrate when the sample is too thin. The TEM sample was kept under vacuum and cleaned in an Ibss GV10x DS Asher plasma cleaner for 10 minutes under 20 W to remove contaminations before being inserted into the TEM column.

A Thermo-Fisher Titan STEM equipped with a CEOS probe aberration corrector operated at 200 kV was used to collect STEM data. A 24.5 mrad semi convergence angle and an 18.9 pA current probe was used. A Gatan BF/ABF detector with 5.7 mrad and 22.8 mrad inner and outer collection angle was used to collect the annular bright field (ABF) images.

[1] S. S. Hong, M. Gu, M. Verma, V. Harbola, B. Y. Wang, D. Lu, A. Vailionis, Y. Hikita, R. Pentcheva, J. M. Rondinelli, et al., Science **368**, 71 (2020).

[2] D. Halliday, J. Eggleston, K. Lee, J. Frost, and S. Beaumont, Solid state communications **96**, 359 (1995).

[3] D. Fang, C. Striemer, T. Gaborski, J. McGrath, and P. Fauchet, Journal of Physics: Condensed Matter **22**, 454134 (2010).

[4] J. Snyder, A. Clark Jr, D. Fang, T. Gaborski, C. Striemer, P. Fauchet, and J. McGrath, Journal of membrane science **369**, 119 (2011).

[5] M. M. Roberts, L. J. Klein, D. E. Savage, K. A. Slinker, M. Friesen, G. Celler, M. A. Eriksson, and M. G. Lagally, Nature materials **5**, 388 (2006).

[6] N. Levy, S. Burke, K. Meaker, M. Panlasigui, A. Zettl, F. Guinea, A. C. Neto, and M. F. Crommie, Science **329**, 544 (2010).

[7] D. Ji, S. Cai, T. R. Paudel, H. Sun, C. Zhang, L. Han, Y. Wei, Y. Zang, M. Gu, Y. Zhang, et al., Nature **570**, 87 (2019).

[8] D. Lu, D. J. Baek, S. S. Hong, L. F. Kourkoutis, Y. Hikita, and H. Y. Hwang, Nature materials **15**, 1255 (2016).

[9] R. De Groot, F. Mueller, P. Van Engen, and K. Buschow, Physical Review Letters **50**, 2024 (1983).

[10] T. Graf, C. Felser, and S. S. Parkin, Progress in solid state chemistry **39**, 1 (2011).

[11] J. Tobola, J. Pierre, S. Kaprzyk, R. Skolozdra, and M. Kouacou, Journal of Physics: Condensed Matter **10**, 1013 (1998).

[12] I. Takeuchi, O. Famodu, J. Read, M. Aronova, K.-S. Chang, C. Craciunescu, S. Lofland, M. Wuttig, F. Wellstood, L. Knauss, et al., Nature materials **2**, 180 (2003).

[13] J. Dong, J. Xie, J. Lu, C. Adelmann, C. Palmstrøm, J. Cui, Q. Pan, T. W. Shield, R. D. James, and S. McKernan, Journal of Applied Physics **95**, 2593 (2004).

[14] J. K. Kawasaki, APL Materials **7**, 080907 (2019).

[15] C. Shekhar, N. Kumar, V. Grinenko, S. Singh, R. Sarkar, H. Luetkens, S.-C. Wu, Y. Zhang, A. C. Komarek, E. Kampert, et al., Proceedings of the National Academy of Sciences **115**, 9140 (2018).

[16] Z. Liu, L. Yang, S. Wu, C. Shekhar, J. Jiang, H. Yang, Y. Zhang, S. Mo, Z. Hussain, B. Yan, et al. (2016).

[17] J. A. Logan, S. Patel, S. D. Harrington, C. Polley, B. D. Schultz, T. Balasubramanian, A. Janotti, A. Mikkelsen, and C. J. Palmstrøm, Nature communications **7**, 1 (2016).

[18] K. Rana, O. Meshcheriakova, J. Kübler, B. Ernst, J. Karel, R. Hillebrand, E. Pippel, P. Werner, A. Nayak, C. Felser, et al., New Journal of Physics **18**, 085007 (2016).

[19] L. Wollmann, A. K. Nayak, S. S. Parkin, and C. Felser, Annual Review of Materials Research **47**, 247 (2017).

[20] M. Hirschberger, S. Kushwaha, Z. Wang, Q. Gibson, S. Liang, C. A. Belvin, B. A. Bernevig, R. J. Cava, and N. P. Ong, Nature materials **15**, 1161 (2016).

[21] S. Chadov, X. Qi, J. Kübler, G. H. Fecher, C. Felser, and S. C. Zhang, Nature materials **9**, 541 (2010).

[22] D. Du, A. Lim, C. Zhang, P. J. Strohbeen, E. H. Shourov, F. Rodolakis, J. L. McChesney, P. Voyles, D. C. Fredrickson, and J. K. Kawasaki, APL Materials **7**, 121107 (2019).

[23] N. P. Butch, P. Syers, K. Kirshenbaum, A. P. Hope, and J. Paglione, Physical Review B **84**, 220504 (2011).

[24] F. Tafti, T. Fujii, A. Juneau-Fecteau, S. R. de Cotret, N. Doiron-Leyraud, A. Asamitsu, and L. Taillefer, Physical Review B **87**, 184504 (2013).

[25] Y. Kim, S. S. Cruz, K. Lee, B. O. Alawode, C. Choi, Y. Song, J. M. Johnson, C. Heidelberger, W. Kong, S. Choi, et al., Nature **544**, 340 (2017).

[26] W. Kong, H. Li, K. Qiao, Y. Kim, K. Lee, Y. Nie, D. Lee, T. Osadchy, R. J. Molnar, D. K. Gaskill, et al., Nature materials **17**, 999 (2018).

[27] H. S. Kum, H. Lee, S. Kim, S. Lindemann, W. Kong, K. Qiao, P. Chen, J. Irwin, J. H. Lee, S. Xie, et al., Nature **578**, 75 (2020).

[28] J. Jiang, X. Sun, X. Chen, B. Wang, Z. Chen, Y. Hu, Y. Guo, L. Zhang, Y. Ma, L. Gao, et al., Nature communications **10**, 1 (2019).

[29] R. Rojas Delgado, R. M. Jacobberger, S. S. Roy, V. S. Mangu, M. S. Arnold, F. Cavallo, and M. G. Lagally, ACS applied materials & interfaces **9**, 17629 (2017).

[30] A. C. Ferrari, J. Meyer, V. Scardaci, C. Casiraghi, M. Lazzeri, F. Mauri, S. Piscanec, D. Jiang, K. Novoselov, S. Roth, et al., Physical review letters **97**, 187401 (2006).

[31] D. Graf, F. Molitor, K. Ensslin, C. Stampfer, A. Jungen, C. Hierold, and L. Wirtz, Nano letters **7**, 238 (2007).

[32] L. G. Cançado, A. Jorio, E. M. Ferreira, F. Stavale, C. A. Achete, R. B. Capaz, M. V. d. O. Moutinho, A. Lombardo, T. Kulmala, and A. C. Ferrari, Nano letters **11**, 3190 (2011).

[33] S. C. OHern, C. A. Stewart, M. S. Boutilier, J.-C. Idrobo, S. Bhaviripudi, S. K. Das, J. Kong, T. Laoui, M. Atieh, and R. Karnik, ACS nano **6**, 10130 (2012).

[34] S. S. Roy, R. M. Jacobberger, C. Wan, and M. S. Arnold, Carbon **100**, 1 (2016).

[35] P. Zeller and S. Günther, New Journal of Physics **16**, 083028 (2014).

[36] H. Hattab, A. T. NDiaye, D. Wall, C. Klein, G. Jnawali, J. Coraux, C. Busse, R. van Gastel, B. Poelsema, T. Michely, et al., Nano letters **12**, 678 (2012).

[37] Y. Li, Soft matter **12**, 3202 (2016).

[38] E. Loginova, S. Nie, K. Thürmer, N. C. Bartelt, and K. F. McCarty, Physical Review B **80**, 085430 (2009).

[39] L. B. Biedermann, M. L. Bolen, M. A. Capano, D. Zemlyanov, and R. G. Reifenberger, Physical Review B **79**, 125411 (2009).

[40] F. Jean, T. Zhou, N. Blanc, R. Felici, J. Coraux, and G. Renaud, Physical Review B **88**, 165406 (2013).

[41] L. Meng, R. Wu, L. Zhang, L. Li, S. Du, Y. Wang, and H. Gao, Journal of Physics: Condensed Matter **24**, 314214 (2012).

[42] Y. Cao, V. Fatemi, S. Fang, K. Watanabe, T. Taniguchi, E. Kaxiras, and P. Jarillo-Herrero, Nature **556**, 43 (2018).

[43] D. A. Ruiz-Tijerina and V. I. Fal'ko, Physical Review B **99**, 125424 (2019).

[44] K. Tran, G. Moody, F. Wu, X. Lu, J. Choi, K. Kim, A. Rai, D. A. Sanchez, J. Quan, A. Singh, et al., Nature **567**, 71 (2019).

[45] T. Nishinaga, T. Nakano, and S. Zhang, Japanese journal

of applied physics **27**, L964 (1988).
[46] Y. Ujiie and T. Nishinaga, Japanese Journal of Applied Physics **28**, L337 (1989).
[47] O.-H. Nam, M. D. Bremser, T. S. Zheleva, and R. F. Davis, Applied Physics Letters **71**, 2638 (1997).
[48] Z. Zytkiewicz, J. Domagala, D. Dobosz, and J. Bak-Misiuk, Journal of applied physics **84**, 6937 (1998).
[49] L. Mandeltort and J. T. Yates Jr, The Journal of Physical Chemistry C **116**, 24962 (2012).
[50] R. Bistritzer and A. H. MacDonald, Proceedings of the National Academy of Sciences **108**, 12233 (2011).
[51] H. Park, C. Lim, C.-J. Lee, J. Kang, J. Kim, M. Choi, and H. Park, Nanotechnology **29**, 415303 (2018).